INTERNATIONAL JOURNAL of RENEWABLE ENERGY RESEARCH
J. Guo et al., Vol.16, No.1, March, 2026

Improved Coordinated LVRT Control Strategy for Grid-forming Direct-drive Wind Turbine

Jia Guo*‡, Yanbo Che*, Yijing Chen**

*Department of Electrical Engineering, Tianjin University, Tianjin , China

** China Huaneng Clean Energy Research Institute Technology Co., Ltd., Beijing, China

(guojia_7@tju.edu.cn, ybche@tju.edu.cn, yj_chen@qny.chng.com.cn)

‡Corresponding Author; Yanbo Che, Postal address, ybche@tju.edu.cn

Received:01.14.2024 Accepted:03.02.2024

Abstract- For grid-forming permanent magnet direct-drive wind turbines during low-voltage ride-through (LVRT), this paper analyses the impact of grid-forming wind turbines on the system, to address the challenge of low wind energy utilization and limited flexibility. A improved coordinated LVRT control strategy involving variable power tracking and rotor overspeed is proposed, which flexibly switches control modes based on the state of the energy storage by combining hybrid energy storage and virtual synchronous generator control. During fault ride-through, the hybrid energy storage module is utilized to store unbalanced energy. When the energy storage capacity is in the warning interval, variable acceleration overspeed is applied to the turbine speed to moderate unbalanced energy and slow down the charging speed, ensuring that the hybrid energy storage power remains in the safety interval. This strategy effectively enhances the LVRT capability and energy utilization of grid-forming units. The correctness of the proposed strategy is verified using the MATLAB/Simulink simulation platform.

Keywords Grid-forming wind turbine, LVRT, hybrid energy storage, variable power tracking; coordinated control.

1. Introduction

As new energy sources are gaining prominence in the energy mix, wind power has received widespread attention for its cleanliness and flexibility[1, 2]. However, as access and installed capacity of wind power gradually increase, the issue of fault ride-through becomes more significant[3-5]. Especially in recent years, the popularity of grid-forming inverters[6] has further expanded the impact of grid faults on wind power generation systems. Many countries have specific regulations governing the LVRT features of wind power systems. These regulations require the systems to operate within a specific range of grid voltage without any disconnection from the grid[7, 8]. If there are sudden changes in the grid voltage, back-to-back transformers cannot entirely link the wind turbine generator (WTG) output power to the grid. This situation arises because the capacity of the grid-side inverter restricts a portion of the energy from the input machine-side rectifier, accumulating on the DC side and resulting in overvoltage as the main fault hazard on that side[9]. Hence, fault traversal is essential to address a range of issues, including energy imbalance between the machines and the power grid. Studying the mechanism leading to system instability is crucial.

Reference [10-11] adopts the traditional chopper circuit and its coordinated control strategy. Unloading resistors are connected in parallel on the DC side to discharge excess active power. This method compensates for the limitation of slow response and poor control from pitch angle control and enhances the control of DC voltage, but the single use of resistor discharge not only causes energy waste, but also imposes higher requirements on the heat resistance capability of the equipment. Reference [12] proposes an LVRT strategy utilizing frozen power loops and a virtual impedance design that is quantitatively analysed in conjunction with modern virtual synchronous generator technology. This approach maintains stable power angles, prevents overcurrent, and provides reactive power support during LV faults. However, the strategy's ability to dissipate unbalanced power during faults to maintain DC-side voltage stability remains to be verified by subsequent experiments. Reference [13] begins to explore the use of supercapacitors to temporarily store excess power generated during failures. Reference [14, 15], focusing on the energy storage system, consider its capacity limitation and propose an improved LVRT control strategy by

combining the energy storage link with the crowbar circuit. These two papers offer a promising research direction to enhance the LVRT capability of wind turbines through combining the benefits of the energy storage link with other control strategies. However, there is also an issue regarding the upper limit of power leakage through the crowbar circuit, which has not fundamentally addressed the power imbalance. Reference [16] proposes a ride-through strategy for low voltage that takes into account rotor inertia and pitch angle control. This approach employs a fuzzy control method to coordinate the supercapacitor with the pitch angle, resulting in decreased energy storage system design expenses. Nevertheless, it also exhibits inadequate control of the grid-side output and significant system oscillations when the control approach is switched. For doubly fed induction generators, reference [17] proposes a method for configuring energy storage and hybrid grid-forming/following reconfiguration converter architecture to address stability issues during faults. However, it overlooks the adverse effect of remaining energy storage capacity on low-voltage ride-through capability.

In summary, the current fault ride-through strategies for grid-forming wind turbines cannot simultaneously address the issues of LVRT, flexible control of energy storage links, and coordinated control when energy storage capacity is limited. Building on this, the paper first aims to enhance the LVRT capability of grid-forming wind turbines by employing a hybrid energy storage system and adjusting the VSG reference value after faults. Subsequently, with the objective of maximizing the utilization of energy storage component capacity while ensuring safety during LVRT, a control strategy based on variable speed coefficient is proposed for the coordinated operation of rotor overspeed and energy storage.

2. Topology and Conventional Control Strategies for Grid-Forming Wind Turbine Systems

2.1. Overall Topology

The topology of the wind power system of the grid-forming permanent magnet direct-drive synchronous generator is shown in Fig.1. Specifically, the wind turbine, via the back-to-back converter (comprising machine-side rectifier, DC-side capacitor, grid-side inverter), generates initially unstable alternating current, undergoes AC-DC-AC conversion, passes through a filter for stabilization, and ultimately transforms into a stable grid-connected alternating current.

2.2. Converter Control Strategy

2.2.1 Conventional grid-side converter control strategy

To address the problem of weak active control link of grid-side converter, virtual synchronous generator (VSG) control is introduced. The VSG control simulates the control of synchronous generator, which consists of virtual governor and virtual excitation controller[18]. Among them, the virtual governor is responsible for the decoupling control of the active loop, which can independently regulate the output active and provide frequency support through the virtual inertia link to optimize the grid performance. According to the synchronous generator rotor motion characteristic equation, the active power control equation of VSG control strategy is:

$$J\omega_0 \frac{\mathrm{d}\omega}{\mathrm{d}t} = P_\mathrm{m} - P_\mathrm{G} - D\omega_0(\omega - \omega_0) \tag{1}$$

Where: J is the virtual inertia of the VSG, which is used to simulate the rotational inertia of the synchronous generator rotor; D is the virtual damping of the VSG, which is used to prevent the sudden change of rotational speed; P_m is the virtual mechanical power inputted to the inverter; P_G is the actual power outputted from the inverter; ω and ω_0 are the actual and rated angular frequencies of the virtual rotor of the VSG.

To enable the inverter to respond to frequency changes, a frequency droop term is incorporated into the control link:

$$P_\mathrm{m} = P_\mathrm{ref} + K_\omega(\omega_0 - \omega) \tag{2}$$

Where: P_ref is the reference value of the inverter output power; K_ω is the frequency droop factor.

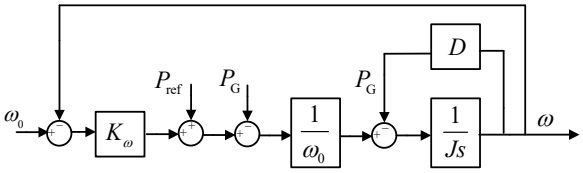

Fig. 2. Active-frequency droop control.

The reactive voltage control equation is shown in equation (3), which is equivalent to the excitation control of the synchronous generator and plays a role in regulating the output voltage of the inverter. To ensure the active power output capability, the reactive power reference value is 0.

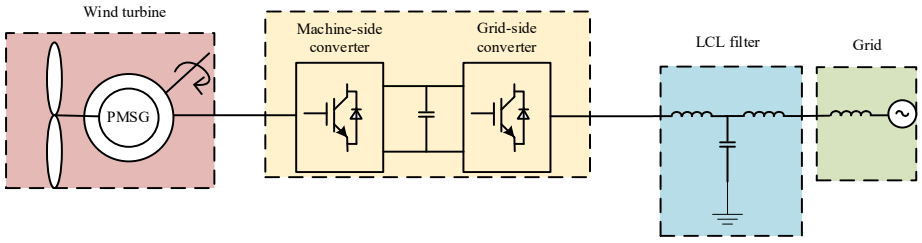

Fig. 1. Grid-forming direct-drive wind power system.

$$E_{\text{ref}} = U_0 + K_u\left(Q_{\text{ref}} - Q_{\text{G}}\right) \tag{3}$$

Where: E_{ref} is the reference voltage magnitude, U_0 is the rated voltage magnitude at the stator terminal of the VSG; Q_{ref} is the reference value of reactive power, while Q_{G} is the actual output value; K_u is the droop factor for reactive-voltage control.

Represented as a control block diagram:

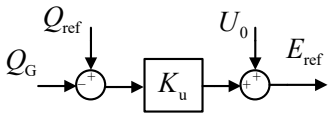

Fig. 3. Reactive power droop control.

2.2.2 Conventional machine-side converter control strategy

The conventional control strategy for the machine-side rectifier involves decoupled vector control based on rotor magnetic field orientation. This strategy uses the rotor magnetic chain direction as the reference direction for the d-axis after park transformation. In this mode, the d-axis current of the generator is maintained at zero. Consequently, the generator's electromagnetic torque is indirectly regulated by transforming the q-axis current to control its active output, known as the zero d-axis current control mode. Accordingly, equation (4) can be transformed into equation (5) [19].

$$\begin{cases} P_{\text{M}} = -\dfrac{3}{2}\left(u_{\text{md}} i_{\text{md}} + u_{\text{mq}} i_{\text{mq}}\right) \\ Q_{\text{M}} = -\dfrac{3}{2}\left(u_{\text{mq}} i_{\text{md}} - u_{\text{md}} i_{\text{mq}}\right) \end{cases} \tag{4}$$

$$P_{\text{M}} = -\frac{3}{2} u_{\text{mq}} i_{\text{mq}} \tag{5}$$

Where: P_{M} is the output active power; Q_{M} is the output reactive power; i_{md} represents the d-axis current component, while i_{mq} represents the q-axis current component; u_{md} represents the d-axis voltage component, while u_{mq} represents the q-axis voltage component.

The q-axis employs a control strategy with a rotational speed outer loop and a current inner loop. This involves calculating the relationship between the rotational speed and output power of the wind turbine at the current wind speed. The optimal rotational speed is determined using the fixed-step-length Paiyama search method. The current rotational speed is then compared with the optimal speed, and the reference value is obtained through the PI controller.

The machine-side converter control strategy is summarized in the block diagram presented in Fig. 4.

In conventional control of grid-connected wind turbines, the machine-side rectifiers solely adjust the reference value of the active loop based on the assessment of whether more power can be generated under the current wind speed conditions. However, this adjustment cannot be made promptly once the DC side is saturated with dissipated power. On the other hand, the grid-side inverter concentrates on the input of active and reactive power into the grid but lacks the capability to respond to voltage dips in the grid. Subsequently, in the following section, the hazards resulting from voltage dips in the system are analysed, and a targeted optimization of the grid-forming control is performed.

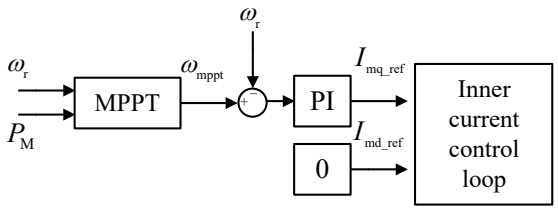

Fig. 4. Machine-side converter control strategy.

3. Impacts And Requirements Under Grid-Side Voltage Dip Faults

3.1. LVRT Specifications

Wind power penetration refers to the percentage of wind power generation relative to the entire power system load [20]. In a system with low wind power penetration, removing small-capacity WTGs from the grid will not impact overall system stability. However, in a system with a high proportion of wind power generators, the shutdown of large-capacity WTGs may lead to secondary effects, such as frequency and voltage collapse [21]. Therefore, Figure 5 clearly illustrates the wind power system's capabilities for LVRT, using China as an example. In the range above the voltage contour line, it is necessary for the wind turbine to be connected to the grid. Especially when the voltage at the grid connection point is below 0.9 p.u., the wind power system needs to possess a certain capability to provide reactive power support.

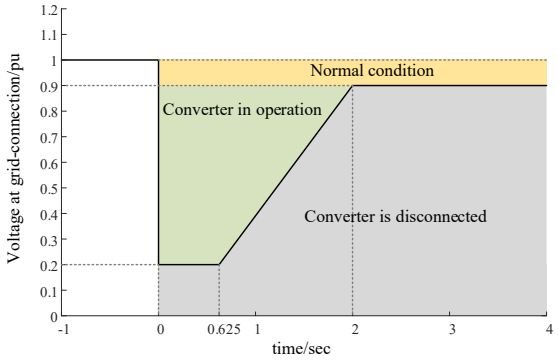

Fig. 5. Technical regulations for LVRT in China.

$$\Delta I_t = K_1 \times (0.9 - U_{\text{G}}) \times I_N, (0.2,, U_{\text{G}},, 0.9) \tag{6}$$

Where: ΔI_t is the reactive current that is injected by the wind power system into the grid during low voltage processes; K_1 is the reactive current ratio coefficient; U_{G} is the grid-connected AC voltage per-unit value; I_N is the rated current of the wind power system.

3.2. Impact of Grid-Side Voltage Dip Faults on the System

WTGs are connected to the grid via back-to-back converters. In the event of a grid-side voltage dip, abnormal conditions like overvoltage and overcurrent may occur within the turbine, potentially leading to turbine disconnection and failure. Ensuring a seamless transition without disconnection during grid-side voltage anomalies is the objective of low-voltage ride-through. Studying the low-voltage ride-through mechanism under conditions that disrupt the unit's stable operating state is crucial for enhancing the control strategy.

(1) Rise of voltage on DC side

During the stable power generation state of WTGs, the power input from the rectifier side of the back-to-back converter equals the power output from the inverter side to the grid.

When the grid voltage suddenly drops, and if the grid-side power reference value remains constant, the grid-side current experiences a sharp increase to ensure power output. However, due to the capacity limitations of the grid-side converter, the output grid current reaches its upper limit, resulting in a decrease in power output. Simultaneously, because of the isolation provided by the back-to-back converter, the turbine side continues to operate in Maximum Power Point Tracking (MPPT) mode, with input power exceeding output power. This isolation effect leads to the turbine side still functioning in MPPT mode, where the input power of the back-to-back converter surpasses the output power, causing a power difference reflected in the increased DC bus capacitor voltage. According to China's LVRT requirements for wind turbines, reactive power must be supplied to the grid to aid voltage recovery, further limiting active current.

$$\Delta P = U_{dc} I_{dc} = P_M - P_G = \frac{1}{2} C \frac{dU_{dc}^2}{dt} \tag{7}$$

Where: ΔP is the power gap between the ports on both sides of the converter; U_{dc} is the DC side voltage; I_{dc} is the DC side current; C is the DC side capacitance.

(2) Rise of fault current

A simplified equivalent circuit for grid-connection is established as shown in Fig. 6.

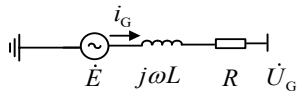

Fig. 6. Simplified equivalent circuit for grid-forming wind turbines.

As seen from the Fig. 6:

$$\dot{E}\text{-}\dot{U}_G = i_G R + L \frac{di_G}{dt} \tag{8}$$

Where: $\dot{E}$ is the inverter output voltage; $\dot{U}_G$ is the grid voltage; i_G is the inverter output current; R and L are the equivalent resistance and reactance of the line between the inverter and the grid, respectively.

Before and after the grid fault, we can approximate that the inverter output voltage maintains a constant amplitude and phase. When the grid voltage dips, the grid-side voltage undergoes changes. Due to the equivalent inductance of the line, the current expression is represented by equation (9).

$$\begin{cases} \Delta U_G = \dot{U}_G(0_-) - \dot{U}_G(0_+) \\ i_G(t) = i_G(0_-) + (1 - e^{-\frac{R}{L}t}) \dfrac{\Delta U_G}{R + j\omega L} \end{cases} \tag{9}$$

Where: ΔU_G is the grid voltage difference before and after the fault; $\dot{U}_G(0_-)$ and $\dot{U}_G(0_+)$ are the grid voltages before and after the fault; $i_G(t)$ is the grid current at time t after the fault; $i_G(0_-)$ is the grid current before the fault.

Neglecting the transient component, the vector magnitude and numerical magnitude of the current are shown in equation (10) and (11).

$$i_G(\infty) = \frac{\dot{E} - \dot{U}_G(0_+)}{R + j\omega L} \tag{10}$$

$$I_G(\infty) = \frac{\sqrt{2}}{|R + j\omega L|} \sqrt{E^2 + U_G^2 - 2EU_G \cos\delta_G} \tag{11}$$

Where: $i_G(\infty)$ is the steady state fault current; $I_G(\infty)$ is its numerical magnitude; δ_G is the phase angle difference between $\dot{E}$ and $\dot{U}_G$.

By examining Eq. (11), it is evident that the fault current is influenced by the phase angle difference between $\dot{E}$ and $\dot{U}_G$. The larger the phase angle difference, the greater the fault current. Consequently, the magnitude of the inverter output fault current can be restricted by controlling the virtual power angle of the VSG during a grid fault.

(3) Deterioration of power angle stability

The dynamic adjustment process of a grid-connected VSG during grid voltage dips unfolds as follows: the reference value of active power during normal VSG operation is represented by P_{ref}, positioning it at point *a* on the power angle characteristic, which is the pre-fault curve. As the grid voltage drops, the operational curve undergoes changes. Due to the inability to abruptly alter the power angle, the operating point swiftly shifts to point *b*, leading to a sudden decline in output power. If not regulated at this point, the output active power will lag behind as the fault characteristic curve rises. If it rises to point *c*, the fault is eliminated, and the power abruptly rises to point d. Following this, the speed decreases from point *d* to point *e*, which is the stable operation point after the fault.

Applying the equal area theorem, in this operation mode, the acceleration area is large, and the maximum deceleration area is small, making system stabilization challenging.

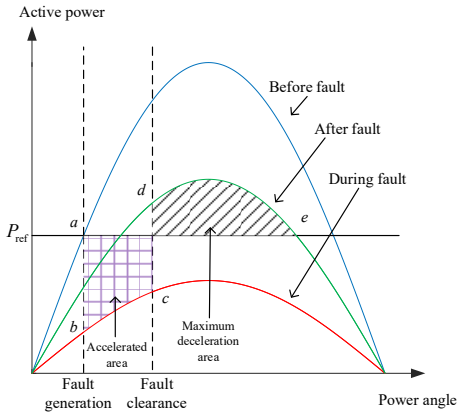

Fig. 7. Power angle characteristic curve for conventional VSG control.

In summary, grid voltage dips result in power imbalance on both sides of the machine network, an increase in fault currents, and a decline in system stability. Consequently, it is imperative to enhance the control strategy during low voltage periods and store the dissipated power difference ΔP to enhance energy utilization.

4. Improved Coordinated Control with LVRT Capability

Building on the grid's voltage dip impacts discussed in the previous section, this paper initially stores and dissipates unbalanced power on both sides of the machine grid through the hybrid energy storage link. Secondly, it adjusts the reference values of active and reactive power of the VSG control during voltage dips to enhance the LVRT capability of the grid-forming wind turbine. Concurrently, a coordinated control of rotor overspeed and hybrid energy storage is proposed, leveraging the remaining capacity of the hybrid energy storage link to maximize wind energy utilization and sustain the health of energy storage elements.

4.1. Improvement of VSG Control Strategy

The proposed improvement method in this paper involves adjusting active and reactive reference values.

According to the regulations, the ratio coefficient of reactive current during LVRT should be not less than 1.5 and not more than 3. In order to ensure a certain active power support capacity during LV ride-through, 1.5 is taken in this paper.

As VSG control indirectly manages reactive current through the control of Q_{ref}, it is essential to transform the demand for reactive current into a demand for reactive power.

$$Q_{\text{ref}} = \sqrt{3}U_{\text{L}} \cdot \Delta I_t = \begin{cases} 0 & 0.9\text{p.u.} \le U_{\text{G}} < 1.1\text{p.u.} \\ 1.5(0.9-U_{\text{G}})\sqrt{3}U_{\text{LN}}I_{\text{N}} & 0.2\text{p.u.} \le U_{\text{G}} < 0.9\text{p.u.} \end{cases} \quad (12)$$

Where: U_{L} is the line voltage output from the inverter, and U_{L} is considered equal to the rated line voltage U_{LN}; I_{N} is the line current output from the inverter.

Considering the inverter prioritizes reactive power output during a fault, the adjustment of active power reference values should account for both power angle stability and the limitations of the inverter's output capacity. The active power output before and after the fault is[22]:

$$P_{\text{N}} = \frac{E_{\text{N}}U_{\text{gN}}\delta_{\text{gN}}}{Z} \quad (13)$$

$$P_{\text{F}} = \frac{E_{\text{F}}U_{\text{gF}}\delta_{\text{gF}}}{Z} \quad (14)$$

Where: E_{N} and U_{gN} are the pre-fault inverter output voltage and grid voltage magnitude, respectively, and δ_{gN} is the pre-fault virtual power angle of the VSG at the steady-state operation point; E_{F} and U_{gF} are the post-fault inverter output voltage and grid voltage magnitude, respectively, and δ_{gF} is the post-fault virtual power angle of the VSG at the steady-state operation point.

Similarly, neglecting the amplitude difference of the inverter output voltage before and after the fault, if the phase angle difference before and after the fault is to be kept unchanged, i.e., $\delta_{\text{gN}} = \delta_{\text{gF}}$, then, according to the principle of power angle stability, the output power of the inverter after the fault should satisfy:

$$P_{\text{F}} = \frac{E_{\text{F}}U_{\text{gF}}\delta_{\text{gF}}}{E_{\text{N}}U_{\text{gN}}\delta_{\text{gN}}}P_{\text{N}} = \frac{U_{\text{gF}}}{U_{\text{gN}}}P_{\text{N}} \quad (15)$$

Assuming that the depth of the grid voltage dip is λ, the post-fault active power reference value should be determined according to the principle of power angle stability after the fault:

$$P_{\text{ref1}} = (1-\lambda)P_{\text{ref0}} \quad (16)$$

Where: P_{ref0} and P_{ref1} are the reference values of VSG active power before and after the fault.

Taking into account the overload capacity of the output current at the grid side, the upper limit of the inverter output current is chosen to be 1.5 times the rated current. Therefore, the upper limit of the active current output with reactive power priority is:

$$i_{d\max} = \sqrt{(1.5i_{\text{N}})^2 - i_q^2} \quad (17)$$

At this point, the upper limit of the active power reference value is:

$$P_{\text{ref2}} = \sqrt{3}(1-\lambda)U_{\text{gN}}\sqrt{(1.5i_{\text{N}})^2 - i_q^2} \quad (18)$$

Considering all factors, the reference value of active power during the fault can be derived as:

$$P_{\text{ref\_fault}} = \min(P_{\text{ref1}}, P_{\text{ref2}}) \tag{19}$$

Following the adjustment of the active power reference value, the deceleration area is partially regulated, as illustrated in Fig. 8.

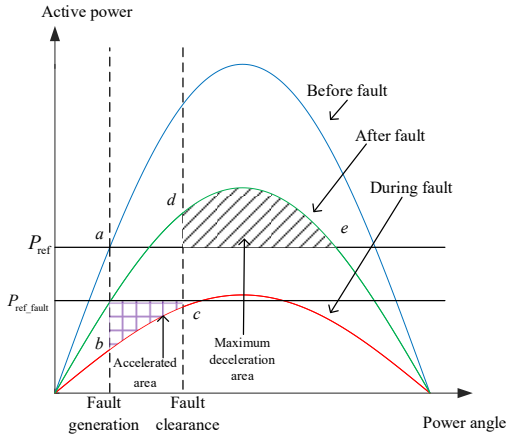

Fig. 8. Power angle characteristic curve for improved VSG control.

Following the adjustment of the reference value, certain constraints are applied to both power angle stability and fault current. Additionally, the issue of abrupt voltage rise on the DC side, resulting from power imbalance after the decrease in active output, still requires resolution.

4.2. Hybrid Energy Storage Control Strategy

The hybrid energy storage unit is connected in parallel to the DC bus via a bidirectional DC/DC converter, and the structure of the bidirectional DC/DC converter is depicted in Figure 9. By managing the on/off state of the two switching tubes, denoted as T_1 and T_2, in the DC/DC converter, the working mode of the energy storage element is controlled.

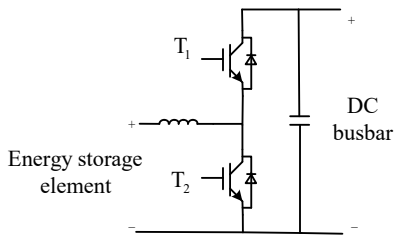

Fig. 9. Bidirectional DC/DC converter structure.

Supercapacitors exhibit fast charging and discharging response times, but their substantial internal resistance results in losses during these processes. They are not suitable for prolonged power supply but are apt for buffering high-frequency power on the DC side. On the other hand, lithium batteries boast greater energy density and are fitting for long-term power supply. However, their response is slower, and there are inherent safety risks associated with overcharging and over-discharging. These risks necessitate careful control of the charging and discharging levels. Lithium batteries are well-suited for extended buffering of low-frequency power on the DC side.

The hybrid energy storage system operates in a constant-current charge/discharge mode, indirectly distributing the power difference by filtering the reference current through a second-order low-pass filter. The control block diagram is depicted in Fig. 5.

$$H(s) = \frac{\omega_{\text{n}}^2}{s^2 + 2\zeta\omega_{\text{n}}s + \omega_{\text{n}}^2} \tag{20}$$

The control block diagram is depicted in Fig. 10. When the DC side voltage deviates from the reference value, the current reference value flowing through the hybrid energy storage system is derived via the PI link. It is then filtered through the low-pass filter to categorize the low-frequency stabilized current component and high-frequency mutated current component as the current reference values for the lithium battery (i_{ref_bat}) and the supercapacitor (i_{ref_sc}), respectively. The difference with the actual values is determined, and subsequently, PI control is implemented to generate the PWM signal for controlling the DC/DC converter.

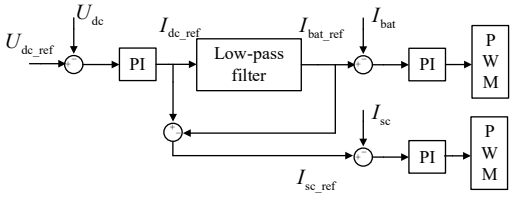

Fig. 10. Energy storage element control block diagram.

The residual capacity of supercapacitors and lithium batteries serves as a crucial foundation for designing control strategies. This is often quantitatively expressed in engineering by the SOC, representing the ratio of the residual capacity to the rated capacity. Given that supercapacitors respond to high-frequency transient components and release energy to aid in active recovery post-fault traversal, the SOC experiences minimal change before and after the fault. Consequently, the control strategy primarily takes into account the SOC state of the lithium battery.

$$SOC_{bat} = 100(1 - \frac{Q_{\text{f}}}{Q_{\text{e}}}) \tag{21}$$

Where: SOC_{bat} is the lithium battery charge state; Q_{f} is the lithium battery discharge; Q_{e} is the lithium battery rated charge.

4.3. Coordinated Control of Rotor Overspeed and Hybrid Energy Storage Based on SOC Capacity

In the event of a symmetrical short-circuit fault with sufficient SOC in the lithium battery (SOC < 70%), the grid-side VSG control adjusts the active reference value. This leads to power imbalance on both sides of the machine network, an upward trend in the DC side voltage, and the hybrid storage voltage control outer loop providing timely feedback on

voltage changes. Consequently, the hybrid storage link is activated to store the imbalance power. At this moment, the grid side maintains the MPPT control to ensure the optimal utilization of wind energy.

As the lithium battery SOC continues to rise, entering the power warning area (70% ≤ SOC < 90%), measures should be taken to ensure the lithium battery operates within a healthy range for prolonged operating life. During this phase, a limitation on power should be imposed by adjusting the rotor speed value in real time. This involves enhancing the speed beyond the maximum power operating point, allowing the imbalance of power to be stored in the rotor of the WTG in the form of kinetic energy. Subsequently, the power input on the turbine side is restricted. In this scenario, determining the turbine speed should prioritize eliminating the power difference based on the degree of imbalance on both sides. According to the wind turbine dynamics equation in equation (22) [23], the power output of the wind turbine at a fixed wind speed and pitch angle can be expressed solely as a function of the rotational speed variable, as illustrated in equation (23).

$$\begin{cases} P_{\mathrm{w}} = \dfrac{1}{2}\rho\pi R^2 V_{\mathrm{w}}^3 C_{\mathrm{p}}(\beta,\lambda) \\ \lambda = \dfrac{\omega_{\mathrm{m}} R}{V_{\mathrm{w}}} \end{cases} \tag{22}$$

$$P_{\mathrm{w}} = f(\omega_{\mathrm{m}}) \tag{23}$$

Where: P_{w} is the output power of wind turbine; ρ is the air density; R is the radius of the turbine blades; V_w is the wind speed; ω_{m} is the WTG rotational speed; $C_{\mathrm{p}}(\beta,\lambda)$ is the wind energy utilization coefficient, which is correlated with the pitch angle β and the tip speed ratio λ.

Utilizing the machine-side power reference value P_{ref}, plug it into formula (22), and identify the unique speed solution ω_{mf} that surpasses optimum speed for current wind speed ω_{mppt}. This speed represents the wind turbine speed value capable of entirely eliminating the power difference through over-speed load shedding control. Approaching the upper limit of the lithium battery power warning zone (SOC=90%), the wind turbine should operate at rotational speed ω_{mf} as much as possible within the safety range to rectify the power difference on both sides. In practical terms, a safety limit $\omega_{\mathrm{m\_max}}$ is imposed on rotor overspeed to safeguard the secure operation of WTG components. This limit $\omega_{\mathrm{m\_max}}$ is commonly set at 1.2 times the rated speed.

$$\omega_{\mathrm{m1}} = \min(\omega_{\mathrm{mf}}, \omega_{\mathrm{m\_max}}) \tag{24}$$

Where ω_{m1} is the upper limit of the speed that should be achieved at SOC = 90%.

As the lithium battery power enters the warning zone, the wind turbine speed should gradually increase in accordance with the rise of SOC. Simultaneously, the rate of speed increase should also gradually escalate with the SOC rise. This ensures that a portion of the wind energy can still be stored and utilized in the hybrid energy storage link at the lower value of the warning zone. Additionally, the wind turbine speed should rise rapidly to prevent battery overcharging as the warning zone value increases. Capitalizing on this characteristic, the paper introduces a variable speed coefficient to control the wind turbine during the LVRT period. This approach transitions the turbine out of the MPPT state once the SOC of the lithium battery enters the power warning zone, initiating variable-rate acceleration

$$\omega_{\mathrm{error}} = k_{\omega}\omega_{\mathrm{m\_ref}} \tag{25}$$

$$k_{\omega} = \begin{cases} 1 & SOC < 70\% \\ \dfrac{a(SOC-70)^2+1}{\omega_{\mathrm{m\_ref}}} & 70\% \le SOC \le 90\% \end{cases} \tag{26}$$

Where: ω_{error} is the reference value of the wind turbine speed during the fault; a is a scaling factor that varies according to the upper speed limit, $a = (\omega_{\mathrm{m1}} - 1)/400$.

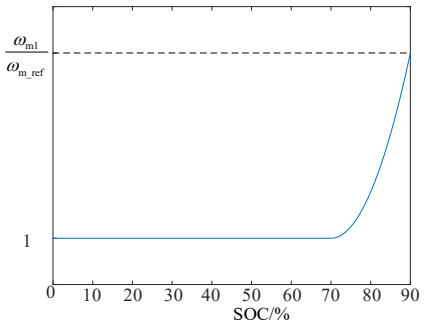

Fig. 11. Variable speed coefficient curve.

In practice, if the wind turbine operating wind speed exceeds the rated wind speed and is already close to the upper speed limit, a condition $\omega_{\mathrm{mf}} > \omega_{\mathrm{m\_max}}$ may arise. In this scenario, the rotor overspeed alone cannot fully decrease the machine-side power to a level sufficient to balance the grid-side output power. Subsequently, after reaching the upper speed limit, a rapid adjustment of the paddle pitch angle is employed to further decrease the wind turbine output power. However, due to the very swift adjustment, the minor power difference continuously dissipated by the hybrid energy storage link during the process is overlooked. The pitch angle adjustment control is illustrated below.

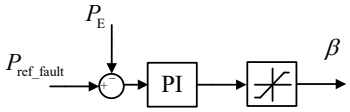

Fig. 12. Block diagram of pitch angle control strategy.

This paper also addresses the issue of lithium battery power discharge. In practical engineering, wind turbines are often operated in MPPT mode for safety reasons. This implies that achieving full power generation may not always be possible. Therefore, the objective of discharging the energy storage can be achieved by controlling the active power

reference value of the grid-side converter at steady state. In a steady state, the active power reference value of the VSG of the grid-side converter is:

$$P_{\text{ref\_steady}} = \begin{cases} P_N & 20\% < SOC, V_{\text{wind}} < V_N \\ P_{\text{M}} & else \end{cases} \quad (27)$$

Where: P_N is the rated power output from the inverter; P_{M} is the power input from the generator to the rectifier converter; V_{wind} and V_N are the current and the rated wind speed.

When the lithium battery power is sufficient (SOC>20%), and the wind speed is lower than the rated wind speed, the rated active power is utilized as the reference value for the grid-side converter output power. The energy from the energy storage link supplements the power difference that persists on the machine side after maximum power tracking. This process, on one hand, discharges excess power in the hybrid storage system, and on the other hand, helps dampen the fluctuation of grid-connected power in the wind power generation system.

In summary, the flowchart of the coordinated control of rotor overspeed and hybrid energy storage based on SOC capacity, proposed in this paper, is shown in Fig. 13.

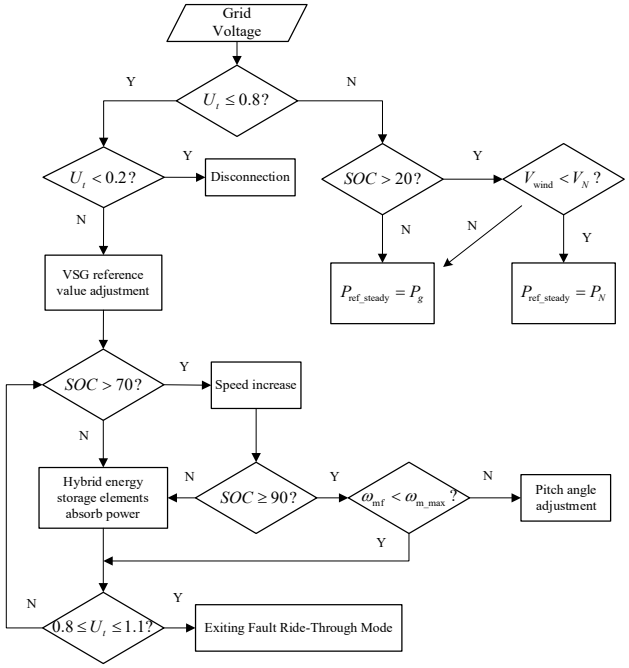

Fig. 13. The LVRT strategy flowchart for coordinating rotor overspeed and SOC proposed in this article.

In this context, disconnection entails the WTG disconnecting from the power grid. If the voltage at the grid connection point drops too low, persisting in grid connection poses a risk to safe operation.

5. Simulation Verification

Using the MATLAB/Simulink simulation platform, we built a 5MW grid-forming, direct-drive wind turbine simulation system. Some of the simulation parameters are presented in Table 1:

Table 1. Simulation parameters

name	value
Turbine capacity/MW	5
DC bus voltage reference value/V	800
DC bus capacitance/mF	17
Li-ion Battery Voltage/V	100
Supercapacitor Voltage/V	100
Supercapacitor Capacity/F	10
Maximum converter current/pu	1.1
Bidirectional DC/DC converter inductors/H	0.355

5.1. Low-Voltage Ride-Through Simulation with Low SOC Value

A three-phase short-circuit fault is initiated at 1s of the simulation run. The voltage drop depth at the parallel network point is approximately 0.3 pu, and the fault duration is 1 s. Selected simulation results are displayed in Fig. 14 and Fig. 15.

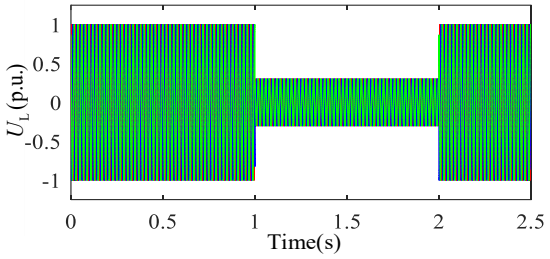

(a) Grid voltage

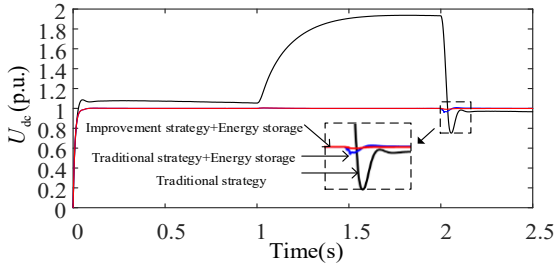

(b) DC side voltage

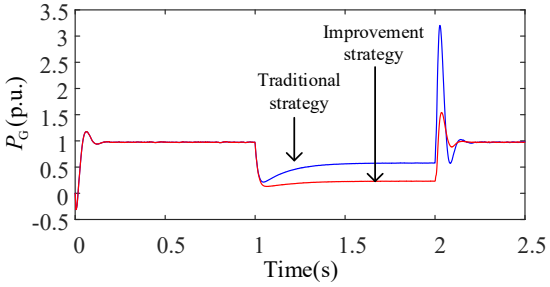

(c) Grid-connected active power

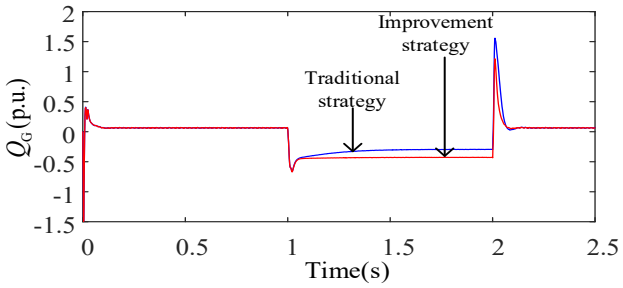

(d) Grid-connected reactive power

Fig. 14. Main waveforms during LVRT.

From Fig. 14(b), it is evident that the hybrid energy storage unit promptly responds to the fault, absorbing unbalanced power from the onset to the end of the low voltage fault. This effectively limits the DC bus voltage, maintaining the DC-side voltage within 0.02 p.u. throughout the fault and recovery phases, meeting the requirements for safe and stable operation of the DC side. Fig. 14(c)(d) displays the active and reactive power waveforms of the turbine with the conventional VSG+hybrid energy storage control strategy and the turbine with the control strategy presented in this paper when connected to the grid, respectively. It is noticeable that, after adopting the control strategy presented in this paper, the active and reactive power output from the grid side can quickly reach the specified values, with a short transition time. Simultaneously, effective control of the power angle during the fault period leads to significantly smaller power fluctuations in the inverter output under the control strategy presented in this paper after the fault is resolved, mitigating the impact on the power grid.

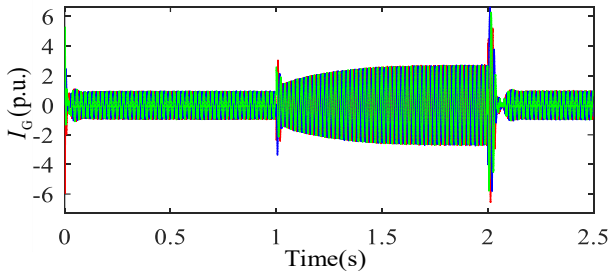

(a) Conventional VSG control strategy

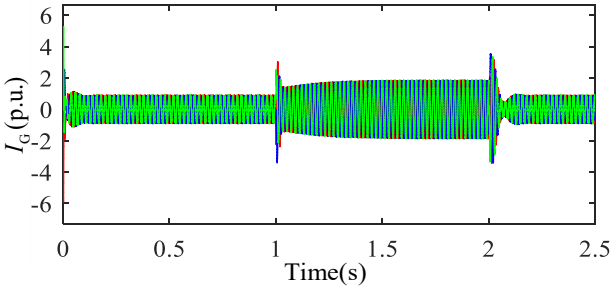

(b) Conventional VSG + hybrid energy storage control strategy

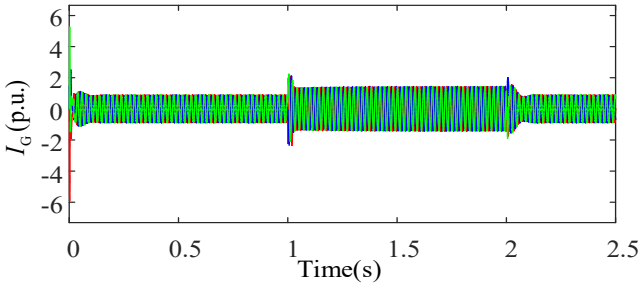

(b) Control strategy of this paper

Fig. 15. Grid-connected current comparison.

According to Fig. (15), the comparison of three-phase currents at the grid-connected point reveals a limited buffering effect of the hybrid storage link on the grid-connected current. The maximum value of the current stabilizes at 1.84 p.u., which still exceeds the safety threshold (1.5 p.u.) in the case of the fault steady state. After adopting the control strategy proposed in this paper, the current at the instant of fault occurrence and recovery is somewhat restricted, and the maximum value of steady-state fault current is limited to below 1.45 p.u., meeting safety requirements and verifying the effectiveness of the strategy proposed in this paper.

5.2. Low-Voltage Ride-Through Simulation with High SOC Values

A three-phase short-circuit fault is initiated at 1s of the simulation run, with a voltage drop depth of about 0.3pu at the parallel network point and a fault duration of 1s. The initial SOC of the lithium battery is set to 70%, and the wind turbine operates at rated wind speed. Some of the simulation results are presented in Fig. 16.

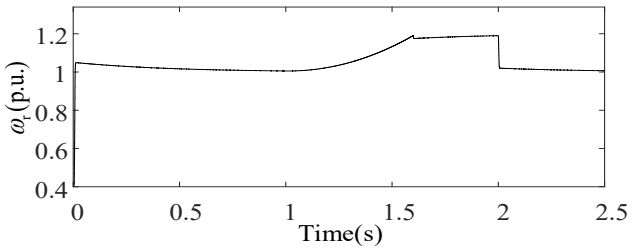

(a) Rotation speed

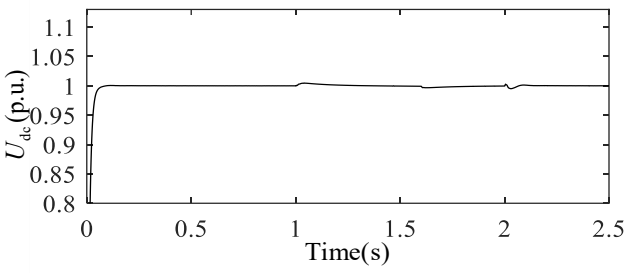

(b) DC side voltage

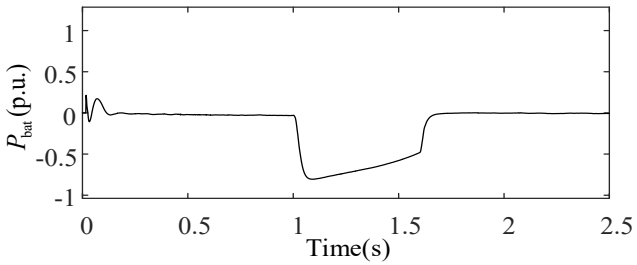

(c) Active power output from lithium batteries

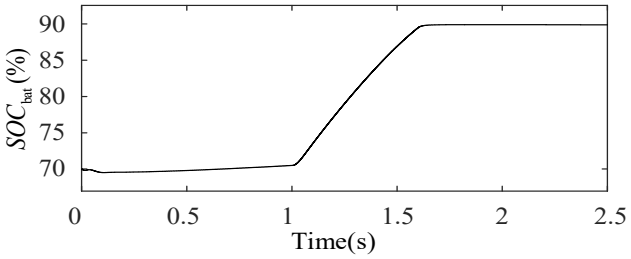

(d) SOC of lithium battery

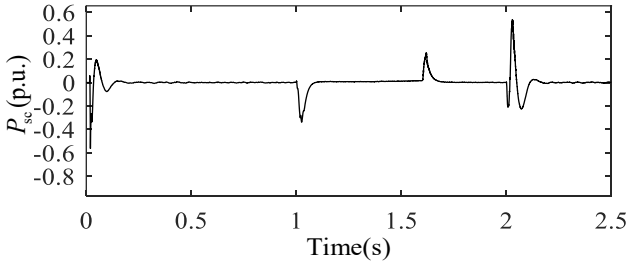

(e) Active power output from supercapacitor

Fig. 15. Main waveforms during LVRT.

In Fig. 15(a), a voltage drop fault occurs on the grid side at 1s. Considering the Li-ion battery SOC state at this time, it has entered the power alert zone, prompting an increase in the wind turbine speed to reduce power output. Around 1.6s, the speed reaches the upper limit, and the paddle pitch angle is adjusted to further reduce the power. The hybrid energy storage system's state, as depicted in Fig. 15(c)(d)(e), shows the effective response of the supercapacitor to high-frequency transient power, buffering the voltage drop and releasing power to aid in recovery when the voltage is restored. The lithium battery rises with the SOC and variable acceleration of rotational speed, and the power buffering gradually slows down. At the upper limit of the SOC (around 1.6s), power is balanced on both sides of the machine network, and the lithium battery enters standby mode, no longer absorbing power. The DC side voltage fluctuation is consistently limited to ±0.02 pu throughout the process. The control mode can be flexibly switched based on the SOC state of the lithium battery, reducing the cost of the hybrid energy storage link and better limiting power fluctuations.

6. Conclusion

This paper initiates an analysis of the fault characteristics associated with grid-type wind turbines during low-voltage ride-through. It introduces a coordinated control strategy addressing rotor overspeed and hybrid energy storage, utilizing the hybrid energy storage SOC capacity. This method tackles challenges like current overrun, unregulated DC voltage, and power angle destabilization resulting from voltage dips on the grid side of permanent magnet synchronous wind turbines. In normal operation, the hybrid energy storage component complements and stabilizes wind power. During a voltage dip fault, reactive current is injected into the grid side per protocol, prioritizing the absorption of imbalanced components on both sides of the machine grid by the hybrid energy storage component to maintain DC side voltage stability. If lithium battery power enters the power alert zone, the wind turbine speed is controlled to accelerate with gradually increasing acceleration based on the degree of SOC overrun. Upon reaching the upper limit of rotor speed, the pitch angle is adjusted to contribute to overall safe and stable operation. By simulating and analyzing the unit's operation under low-voltage fault conditions in two SOC states, the effectiveness and reasonableness of the proposed control strategy are confirmed. This strategy can improve the energy utilization rate and streamline the optimal configuration of the hybrid energy storage link's capacity, ensuring safe operation.

Acknowledgements

This paper was supported by the National Key R&D Program of China(2023YFB4204700).

Author Contributions:

J. Guo was responsible for the conceptualization, validation, resources, data curation, software development, and project administration. J.Guo and Y.B.Che jointly contributed to the methodology, formal analysis, investigation, original draft preparation, review and editing, visualization. Y.J.Chen contributed to the supervision, and funding acquisition. All authors have read and agreed to the published version of the manuscript.

Conflict of Interest:

The author(s) declared no potential conflicts of interest with respect to the research, authorship, and/or publication of this article.

References

[1] S. Jadidi, H. Badihi, and Y. Zhang, “Enhancing hierarchical fault-tolerant cooperative control in wind farms: The application of model predictive control and control reallocation,” in Proc. 2023 12th Int. Conf. on Renewable Energy Research and Applications (ICRERA), 4–7 June 2023, pp. 429–434.

[2] Y.A. Eldahab, N.H. Saad, and A. Zekry, “Assessing wind energy conversion systems based on newly developed wind turbine emulator,” International Journal of Smart Grid, vol. 4, no. 4, pp. 127–139, 2020.

[3] E. El Hawatt, M.S. Hamad, K.H. Ahmed, and I.F. El Arabawy, "Low voltage ride-through capability enhancement of a DFIG wind turbine using a dynamic voltage restorer with adaptive fuzzy PI controller," in Proc. 2013 Int. Conf. on Renewable Energy Research and Applications (ICRERA), 20–23 Oct. 2013, pp. 1234–1239.

[4] Z. Din, J. Z. Zhang, Z. Xu, Y. Q. Zhang, and J. Zhao, "Low voltage and high voltage ride-through technologies for doubly fed induction generator system: Comprehensive review and future trends," IET Renewable Power Generation, vol. 15, no. 3, pp. 614–630, 2021.

[5] H. Wang, Y. Wang, S. Wang, B. Zhao, and Y. Xing, "High- and low-voltage ride-through control strategy for DFIG wind power system based on variable dynamic voltage command value," High Voltage Engineering, vol. 48, no. 9, pp. 3680–3688, 2022.

[6] C. Busada, S. G. Jorge, and J. A. Solsona, "Current-controlled synchronverter: A grid fault tolerant grid-forming inverter," IEEE Transactions on Industrial Electronics, vol. 71, no. 4, pp. 3233–3241, 2024.

[7] A.Q. Al-Shetwi, M.A. Hannan, K.P. Jern, M. Mansur, and T. M. I. Mahlia, "Grid-connected renewable energy sources: Review of the recent integration requirements and control methods," Journal of Cleaner Production, vol. 253, 2020.

[8] R. Cardenas, R. Pena, S. Alepuz, and G. Asher, "Overview of control systems for the operation of DFIGs in wind energy applications," IEEE Transactions on Industrial Electronics, vol. 60, no. 7, pp. 2776–2798, 2013.

[9] A.A. Ansari and G. Dyanamina, "Fault ride-through operation analysis of doubly fed induction generator-based wind energy conversion systems: A comparative review," Energies, vol. 15, no. 21, 2022.

[10] S. Zhou, Q. Wang, X. Lu, Y. Ni, and M. Xu, "Control strategy of low voltage ride-through for double-fed wind generator with the stator crowbar circuit mode switch," Power System Protection and Control, vol. 45, no. 4, pp. 33–39, 2017.

[11] D.D. Banham-Hall, C. A. Smith, G.A. Taylor, and M.R. Irving, "Meeting modern grid codes with large direct-drive permanent magnet generator-based wind turbines—Low-voltage ride-through," Wind Energy, vol. 15, no. 5, pp. 799–810, 2012.

[12] Y.H. Liu, Y. Wang, H. Liu, L.S. Xiong, M. X. Li, Y. Peng, Z. Xu, and M. H. Wang, "An LVRT strategy with quantitative design of virtual impedance for VSG," International Journal of Electrical Power & Energy Systems, vol. 140, 2022.

[13] S. Hou, Y. Fang, J. Zeng, and Z. Yin, "Application of supercapacitors to improve wind power system's low voltage ride-through capability," Electric Machines and Control, vol. 14, no. 5, pp. 26–31, 2010.

[14] Y.X. Wang, S.Y. Wang, and L.H. Yang, "Low-voltage ride-through control strategy of permanent magnetic synchronous wind turbine with coordination of super capacitor energy storage and chopper circuit," High Voltage Apparatus, vol. 59, no. 4, pp. 177–185, 2023.

[15] C. Li, Y. Z. Cao, B. Li, B. Liu, F. Qiao, and P.Y. Chen, "A novel low voltage ride-through scheme for DFIG based on the cooperation of hybrid energy storage system and crowbar circuit," Journal of Energy Storage, vol. 73, 2023.

[16] K.C. and K.W., "Enhanced low-voltage ride-through coordinated control for PMSG wind turbines and energy storage systems considering pitch and inertia response," IEEE Access, vol. 8, pp. 212557–212567, 2020.

[17] D. Song, Q. Xie, Z. Zheng, J. Ren, C. Li, and Y. Wang, "Hybrid grid forming/following reconfiguration converter architecture for DFIG," in Proc. 2023 IEEE Int. Conf. on Applied Superconductivity and Electromagnetic Devices (ASEMD), Tianjin, China, 2023, pp. 1–2.

[18] Y. Zheng, T. Wang, S. He, Y. Wu, Y. Kang, and D. Liu, "Analytical expression of short circuit current for virtual synchronous generator with improved low voltage ride-through control strategy," in Proc. 2023 IEEE Power & Energy Society General Meeting (PESGM), 2023, pp. 1–5.

[19] H. Benbouhenni, H. Gasmi, and N. Bizon, "Direct reactive and active power regulation of DFIG using an intelligent modified sliding-mode control approach," International Journal of Smart Grid, vol. 6, no. 4, pp. 157–172, 2022.

[20] L. Xiang, H. W. Zhu, Y. Zhang, Q. T. Yao, and A. J. Hu, "Impact of wind power penetration on wind–thermal-bundled transmission system," IEEE Transactions on Power Electronics, vol. 37, no. 12, pp. 15616–15625, 2022.

[21] A. isikaer, Y. Zhu, and B. Tang, "Summarizing fault ride-through characteristics of wind turbines," Power System Protection and Control, vol. 41, no. 19, pp. 147–153, 2013.

[22] T. Zheng, Z. Wang, and P. Zou, "Research on low voltage ride-through control strategy of virtual synchronous generator based on phase jump compensation," Power System Technology, vol. 47, no. 1, pp. 100–108, 2023.

[23] A. Belkaid, I. Colak, K. Kayisli, and R. Bayindir, "Modeling of a permanent magnet synchronous generator in a power wind generation system with an electrochemical energy storage," International Journal of Smart Grid, vol. 2, no. 4, pp. 197–202, 2018.